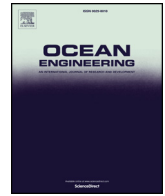




ELSEVIER

Contents lists available at ScienceDirect

Ocean Engineering

journal homepage: www.elsevier.com/locate/oceaneng

Numerical study of flow-induced vibration of a flexible plate behind a circular cylinder

Huakun Wang, Qiu Zhai, Jisheng Zhang*

College of Harbour, Coastal and Offshore Engineering, Hohai University, Nanjing, China

ARTICLE INFO

Keywords:

Flow-induced vibration
Flexible plate
Gap spacing
Bending stiffness
Peak amplitude

ABSTRACT

Flow-induced vibration (FIV) of a flexible plate located in the wake of a rigid circular cylinder is investigated numerically in this study. Computations are performed at two Reynolds numbers $Re = 100$ and 200 , with the plate bending stiffness K_B varying from 0.00563 to 0.36 . The gap spacing between the cylinder and the plate varies within the range of $2.0 \leq S/D \leq 5.0$ (D is the cylinder diameter). Numerical results show that the optimum location with the maximum vibration response is found to be the medium spacing, within which the vortex structures are fully formed in the gap and impinge on the plate successively. The maximum peak amplitude of the tip appears at the smallest K_B where the plate experiences the first- and second-bending motions; accordingly, the orbit of the tip presents a clear “Figure-8” pattern, indicating that the bending deformation has strong nonlinearity. It is also found that there are two mechanisms driving the plate to vibrate in both first- and second-bending modes. The first mechanism is the vortex impingement with the low pressure core, while the second is the high pressure region induced by the stagnation of flow near the turn-up part of the plate.

1. Introduction

A flexible structure immersed in a fluid flow may deform and vibrate owing to the fluid forces acting on its surface. This, in turn, changes the flow field resulting in a coupling process between the fluid and the structure. Over the past few decades, flow-induced vibration (FIV) of a thin flexible structure has received increasing attention due to its importance in applications, such as surgical techniques for snoring (Huang, 1995), paper processing (Watanabe et al., 2002), fish locomotion (Lauder, 2015) and ocean energy harvesting (Jbaily and Jeung, 2015). Although these applications are widespread, the FIV phenomenon still puzzles people due to its complicated coupling dynamics.

As a multi-physics issue, FIV of a thin flexible structure involves the interactions of an elastic body with surrounding fluid flow. The structural deformation and vibration are physically determined by not only the fluid condition but also the material and geometric properties. To obtain the physical insights on the underlying mechanisms, the present model of fluid-structure interaction (FSI) is usually treated as a cantilevered flexible plate placed in an undisturbed uniform flow for scientific research. During the past decades, numerous studies have been performed to deal with this issue (Kornecki et al., 1976; Huang, 1995; Guo and Paidoussis, 2000; Balint and Lucey, 2005; Eloy et al., 2007; Tang and Paidoussis, 2007). The common results predict that the flexible plate suddenly loses stability and attains an intensified flapping

motion beyond a critical flow speed; this change is usually attributed to a broken compromise between the unsteady pressure forces of the fluid and the bending stiffness of the plate. Moreover, Tang and Paidoussis (2009) studied the coupled dynamics of two cantilevered flexible plates aligned parallel to each other in open axial flow. They found that the flapping threshold is a function of the separation between the two plates. The two-plate system can oscillate in both in-phase and out-of-phase modes. A further work by Gurugubelli et al. (2014) noticed that there exists an optimum spacing between the plates for which the flexible plates experience greater resonance amplitude.

Additionally, motivated by the FIV energy harvesting mechanism of the piezoelectric material, quite a few investigations have been conducted on a flexible plate behind a bluff body. Taylor et al. (2001) experimentally demonstrated continuous extraction of electrical energy from a plate made of piezoelectric membrane behind a bluff body, in which an alternative variation of the Kármán vortex street excites periodic flapping of the membrane. Subsequently, Allen and Smits (2001) claimed that the optimal coupling between an energy-harvesting process and the wake flow is best defined as a resonance condition in which the membrane has a negligible damping effect on the original Kármán vortex street. Lee and You (2013) numerically analyzed the vortex-shedding-induced vibration of a splitter plate fixed to the lee side of a fixed circular cylinder. The results documented that the deflection shape of a splitter plate is dependent on the length of the plate,

* Corresponding author.

E-mail address: jszhang@hhu.edu.cn (J. Zhang).

while the deflection magnitude is a function of the bending stiffness and natural frequency of the corresponding plate. Nayer et al. (2014) performed a complementary experimental-numerical investigation on flow past a cylinder with a trailing flexible plate. They claimed that the ratio of structural density to fluid density has the least effect on the plate response compared with Young's modulus and material thickness. Furquan and Mittal (2015) conducted a preliminary study of flow past two square cylinders with deformable splitter plates. It was found that the two coupled plates initially undergo small amplitude out-of-phase oscillations, but later they settle into in-phase vibrations; when the dominant vibration frequency is close to the structural natural frequency, lock-in occurs for certain values of flexibility. A recent study by Purohit et al. (2018) focused on the influence of flow velocity and flexural rigidity on FIV of a flexible plate attached to a square bluff body. The results present a nonlinear relation between vibration level and flow velocity as well as structural flexibility. For a particular combination of flow velocity and plate stiffness, the coupled fluid-structure system shows resonance condition. All the configurations mentioned above are closely associated with an extraneously induced excitation, which is characterized by the unsteady pressure force due to the vortex shedding from the upstream bluff body (Allen and Smits, 2001; Lee and You, 2013). However, little research has been performed on the influence of the bluff body on the vortex shedding near the critical gap spacing, beyond which the plate response may differ significantly.

In this study, flow past a rigid circular cylinder with an unattached flexible plate is investigated numerically. The plate is located in the cylinder wake, and the gap spacing is defined as the distance between the trailing point of the cylinder and the leading point of the plate. A series of numerical calculations are performed by using a strongly coupled finite element model. This study aims at exploring the effects of both gap spacing and bending stiffness on the modification of vortex shedding and the FIV behavior of the plate. Particular attention is paid to the vibration amplitude, the frequency characteristics, and the dynamic mechanisms behind the vortex-plate interactions.

The remainder of this paper is organized as follows. Section 2 describes the details of the computational methodology. It is followed by the numerical validation in Section 3 and the problem definition in Section 4. Section 5 presents the numerical results of FIV of the flexible plate behind the cylinder. Finally, concluding remarks are drawn in Section 6.

2. Numerical methods

2.1. Computational fluid dynamics (CFD)

The governing equations for the incompressible fluid flow are the Navier-Stokes (NS) equations and the continuity equation. In this study, the Arbitrary Lagrangian-Eulerian (ALE) scheme (Donea et al., 1982) is adopted to deal with the moving boundaries. The NS equations and the continuity equation in ALE form can be written as:

$$\rho_f \frac{\partial \mathbf{u}_f}{\partial t} + \rho_f ((\mathbf{u}_f - \mathbf{u}_m) \cdot \nabla) \mathbf{u}_f = \nabla \cdot (\boldsymbol{\sigma}_f) \quad (1)$$

$$\nabla \cdot \mathbf{u}_f = 0 \quad (2)$$

In the above equations, ρ_f is the density of the fluid, \mathbf{u}_f is the fluid velocity, t is the time, and \mathbf{u}_m is the mesh velocity computed by solving a modified Laplace equation (Wang et al., 2014) in this study. The fluid stress tensor $\boldsymbol{\sigma}_f$ is defined as:

$$\boldsymbol{\sigma}_f = -p\mathbf{I} + \rho_f \nu_f (\nabla \mathbf{u}_f + (\nabla \mathbf{u}_f)^T) \quad (3)$$

where p is the pressure, \mathbf{I} is the identity tensor, and ν_f is the kinematic viscosity of the fluid.

The temporal discretization of the NS equation is performed by the semi-implicit four-step fractional method. The streamline upwind/

Petrov-Galerkin (SUPG) finite element scheme is applied to the spatial discretization. More details about the solution of the NS equation can be found in Wang et al. (2014).

2.2. Computational structural dynamics (CSD)

Deformation of the flexible structure is governed by the equation of momentum conservation, which reads as follows:

$$\rho_s \ddot{\mathbf{u}}_s = \nabla \cdot \boldsymbol{\sigma}_s + \rho_s \mathbf{f} \quad (4)$$

where ρ_s is the structural density, \mathbf{u}_s is the displacement, $\boldsymbol{\sigma}_s$ is the Cauchy stress tensor, and \mathbf{f} denotes the body force. By assuming a Saint Venant-Kirchhoff material, the constitutive equation can be written using the 2nd Piola-Kirchhoff stress tensor \mathbf{S} and the Green-Lagrange strain tensor \mathbf{E} :

$$\mathbf{S} = \frac{\nu_s E}{(1 + \nu_s)(1 - 2\nu_s)} (\text{tr} \mathbf{E}) \mathbf{I} + \frac{E}{1 + \nu_s} \mathbf{E} \quad (5)$$

where ν_s is the Poisson ratio and E is the Young's modulus. \mathbf{S} is related to $\boldsymbol{\sigma}_s$ through geometric transformation:

$$\mathbf{S} = J \mathbf{F}^{-1} \boldsymbol{\sigma}_s \mathbf{F}^{-T} \quad (6)$$

where \mathbf{F} is the deformation gradient tensor, and J is the determinant of \mathbf{F} .

By the principle of virtual work, Eq. (4) can be recast in a weak variational form:

$$\int_{\Omega} \rho_s \frac{\partial^2 \mathbf{u}_s}{\partial t^2} \cdot \delta \mathbf{u}_s d\Omega + \int_{\Omega} \mathbf{S} : \delta \mathbf{E} d\Omega = \int_{\Omega} \rho_s \mathbf{f} \cdot \delta \mathbf{u}_s d\Omega + \int_{\Gamma} \mathbf{t}_f \cdot \delta \mathbf{u}_s d\Gamma \quad (7)$$

where $\delta \mathbf{u}_s$ and $\delta \mathbf{E}$ are the virtual displacement and strain, respectively, and \mathbf{t}_f denotes the fluid traction on the fluid-structure interface Γ . The finite element discretization of Eq. (7) is performed by introducing a vector of nodal displacements \mathbf{d} , which satisfies $\mathbf{u}_s^e = \mathbf{N} \mathbf{d}^e$, where \mathbf{N} is the displacement interpolation matrix in an element e . Eq. (7) in the matrix-vector form is then obtained as follows:

$$\mathbf{M} \ddot{\mathbf{d}}^{t+\Delta t} + \mathbf{K}_T^t (\mathbf{d}^{t+\Delta t} - \mathbf{d}^t) = \mathbf{Q}^{t+\Delta t} - \mathbf{F}^{t+\Delta t} \quad (8)$$

where

$$\begin{aligned} \mathbf{M} &= \sum_e \int_{\Omega_e} \rho_s \mathbf{N}^T \mathbf{N} d\Omega, \quad \mathbf{K}_T^t = \sum_e \int_{\Omega_e} ((\mathbf{B}_L^t)^T \mathbf{D} \mathbf{B}_L^t + (\mathbf{B}_{NL}^t)^T \mathbf{S}^t \mathbf{B}_{NL}^t) d\Omega \\ \mathbf{Q}^{t+\Delta t} &= \sum_e \int_{\Omega_e} \rho_s \mathbf{N}^T \mathbf{f}^{t+\Delta t} d\Omega + \sum_e \int_{\Gamma_e} \mathbf{N}^T \mathbf{t}_f^{t+\Delta t} d\Gamma, \\ \mathbf{F}^{t+\Delta t} &= \sum_e \int_{\Omega_e} (\mathbf{B}_L^{t+\Delta t})^T \mathbf{S}^{t+\Delta t} d\Omega \end{aligned} \quad (9)$$

In the above equations, \mathbf{M} is the mass matrix, \mathbf{K}_T is the tangent stiffness matrix, \mathbf{Q} characterizes the vector of fluid load acting on the structure (pressure and shear stress), \mathbf{F} is the vector of internal nodal force, \mathbf{B}_L and \mathbf{B}_{NL} are the linear and nonlinear strain-displacement transformation matrices, respectively, \mathbf{D} is the elasticity matrix, and \mathbf{S} is the 2nd Piola-Kirchhoff stress vector. Applying the Newmark- β method (Newmark, 1959) for time integration and the modified Newton-Raphson method (Bathe et al., 1975) for geometrically nonlinear analysis, Eq. (8) is solved as:

$$\left(\mathbf{K}_T^t + \frac{1}{\alpha \Delta t^2} \mathbf{M} \right) \Delta \mathbf{d}^{(k)} = \mathbf{Q}^{t+\Delta t} - \mathbf{F}^{t+\Delta t(k)} - \mathbf{M} \left[\frac{1}{\alpha \Delta t^2} (\mathbf{d}^{t+\Delta t(k)} - \mathbf{d}^t) - \frac{1}{\alpha \Delta t} \dot{\mathbf{d}}^t - \left(\frac{1}{2\alpha} - 1 \right) \ddot{\mathbf{d}}^t \right] \quad (10)$$

$$\begin{aligned} \mathbf{F}^{t+\Delta t(0)} &= \mathbf{F}^t, \quad \mathbf{d}^{t+\Delta t(0)} = \mathbf{d}^t, \\ \mathbf{d}^{t+\Delta t(k+1)} &= \mathbf{d}^{t+\Delta t(k)} + \Delta \mathbf{d}^{(k)} \quad (k = 0, 1, 2, \dots) \end{aligned} \quad (11)$$

In the above algorithm, k is the iteration counter, $\Delta \mathbf{d}$ is the vector of displacement increment in per iteration step, and α is the implicitly controlled weighting value which is set to 0.25. The parameter β is not

Download English Version:

<https://daneshyari.com/en/article/8062029>

Download Persian Version:

<https://daneshyari.com/article/8062029>

[Daneshyari.com](https://daneshyari.com)